大腿骨近位部骨折用髄内釘の金属方向と周波数エンコード傾斜磁場の方向は，磁化率アーチファクトの出現に影響を与える ： open MRI を用いた検討（英文）

竹内，直英
九州大学大学院医学研究院整形外科

光安，廣倫
九州大学大学院医学研究院整形外科

仲西，知憲
九州大学大学院医学研究院整形外科

西村，須磨子
日立メディコ株式会社アプリケーション部

他

https://doi.org/10.15017/19871

出版情報：福岡醫學雜誌. 102 (5), pp.185-194, 2011-05-25. 福岡医学会
バージョン：
権利関係：

Original Article

The Orientation of Orthopaedic Metallic Devices Relative to the Frequency-Encoding Gradient Affects Susceptibility Artifacts : An Experiment Using Open MR Imaging

Naohide Takeuchi[1)], Hiromichi Mitsuyasu[1)], Tomonori Nakanishi[1)], Sumako Nishimura[2)], Takeshi Shimoto[3)], Hidehiko Higaki[3)], Makoto Hashizume[4)] and Yukihide Iwamoto[1)]

[1)]*Department of Orthopaedic Surgery, Graduate School of Medical Sciences, Kyushu University, Fukuoka*
[2)]*Clinical Application Department Marketing Division, Hitachi Medical Co. Ltd.*
[3)]*Department of Biorobotics, Faculty of Engineering, Kyushu Sangyo University, Fukuoka*
[4)]*Department of Advanced Medical Initiatives, Faculty of Medical Sciences, Kyushu University, Fukuoka*

Abstract Purpose : To evaluate the magnetic susceptibility artifacts associated with different frequency-encoding gradient directions for an angled cephalomedullary device of the proximal femur, and to determine the optimal extremity positioning for reducing artifacts using 0.4 T open MR imaging.
Materials and methods : Two different angular devices made of titanium alloy and stainless steel were used. The images were obtained with the frequency-encoding gradient parallel to the rod (Group R) and parallel to the lag screw (Group L). The device positioning was altered in order to obtain images with frequency-encoding gradient parallel to the rod and parallel to the lag screw. The artifact areas associated with the whole device and the lag screw were statistically evaluated.
Results : For both devices, the mean artifact area in Group L was significantly larger than that in Group R ($p < 0.05$). However, the mean artifact area of the lag screw only in Group L was significantly smaller than that in Group R ($p < 0.05$).
Conclusion : Susceptibility artifacts for angled cephalomedullary devices can be minimized when the frequency-encoding gradient is parallel to the long axis of the regions of interest. Open MR imaging enables us to obtain the optimal orientation for minimizing susceptibility artifacts.

Key words : magnetic susceptibility artifacts, frequency-encoding gradient, open MR imaging, angled cephalomedullary device of the proximal femur.

Introduction

Magnetic resonance (MR) imaging has been used routinely and safely in preoperative and postoperative patients with orthopaedic metallic implants. It can be used to provide anatomic evaluation of the femoral head, acetabulum, hip joint, and surrounding structures[1)~3)]. In particular, the value of MR imaging has been demonstrated in cases of infection, tumors, and osteonecrosis of the femoral head. During MR imaging, however, geometric distortion occurs in soft tissues adjacent to ferromagnetic components, such as orthopaedic hardware. This distortion, known as magnetic susceptibility artifact, renders the evaluation difficult and limits the efficacy of MR imaging[4)].

The frequency-encoding gradient is one of the most important factors in reducing susceptibility artifacts. Some studies have demonstrated the optimal devices positioning related to the frequency-encoding gradient in regard to various

Correspondence to :
Hiromichi Mitsuyasu, MD, PhD
3-1-1 Maidashi, Higashi-ku, Fukuoka City, Fukuoka, Japan 812-8582
Tel : + 81-92-642-5488
Fax : + 81-92-642-5507
E-mail : hiro@ortho.med.kyushu-u.ac.jp

devices[4)~10)]. However, there has so far been no research concerning the relationship between the frequency-encoding gradient direction and the artifact area (whole artifact area and the local artifact area of interest) in the angled cephalomedullary device, using open MR imaging.

Our hypothesis is that in the angled cephalomedullary device of the proximal femur, which consists of the main component (short intramedullary rod) and the substitute component (femoral neck lag screw), the local susceptibility artifact occurring around the lag screw will become smaller when the femoral neck lag screw itself is parallel to the frequency-encoding gradient than when the short intramedullary rod is parallel to the frequency encoding gradient.

The purpose of this study was to quantify the magnetic susceptibility artifacts associated with different frequency-encoding gradient directions for an angled cephalomedullary device of the proximal femur, and to determine the optimal extremity positioning for reducing artifacts using open MR imaging.

Materials and Methods

Phantom model

Two different angled cephalomedullary device of the proximal femur were used in our study. One was made of stainless steel (22Cr13Ni5Mn) (Zimmer Inc. Warsaw, Indiana, USA), and the other was made of titanium alloy (TiAl6V4) (DePuy Orthopaedics Inc. Warsaw, Indiana, USA). Both devices are composed of a short intramedullary rod and a femoral neck lag screw (Fig. 1). The central part of the short intramedullary rod was 13 mm in diameter, 18 cm in length, and the femoral neck lag screw was 100 mm in length. In each device, the angle between the rod and the lag screw was 130° . The stainless steel device is composed of iron (55%), chromium (Cr ; 20.5~23.5 %), nickel (Ni ; 11.5~13.5%), manganese (Mn ; 4~6%), molybdenum (Mo ; 2~3%), copper (Cu ; ≦ 0.50%), vanadium (0.1~0.3%), nitrogen (N ; ≦0.2~ 0.4%), phosphorus (P ; ≦ 0.025%), and carbon (C ; ≦ 0.03%). While, the titanium alloy device is composed of titanium (88.48~91.0%), aluminium (Al ; 5.5~6.5%), vanadium (3.5~4.5%), iron (≦0.25 %), oxygen (O_2 ; ≦ 0.13 %), hydrogen (H_2 ; ≦ 0.012 %), carbon (C ; ≦ 0.08%), and nitrogen (N ; ≦0.05 %).

Each device was suspended 10 cm from a wooden bar with the three strings. Each wooden bar was placed at the top of the container (Fig. 2). Both types of devices were placed in a rectangular plastic container filled with the gel phantom

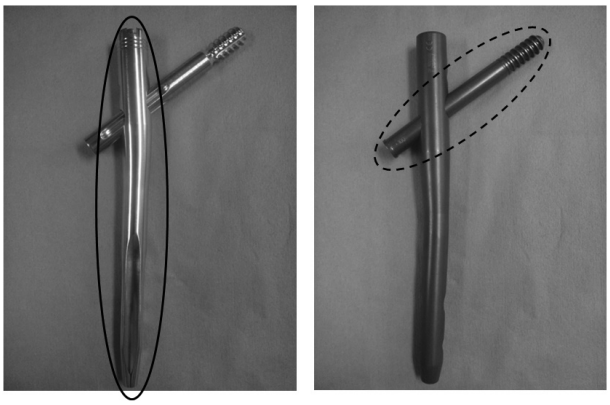

(a) (b)

Fig. 1 Photographs of the angled cephalomedullary device of the proximal femur.
(a) The device made of stainless steel. (b) The device made of titanium alloy. The solid circle is the rod, and the dotted circle is the lag screw. The angle between the rod and the lag screw was 130°.

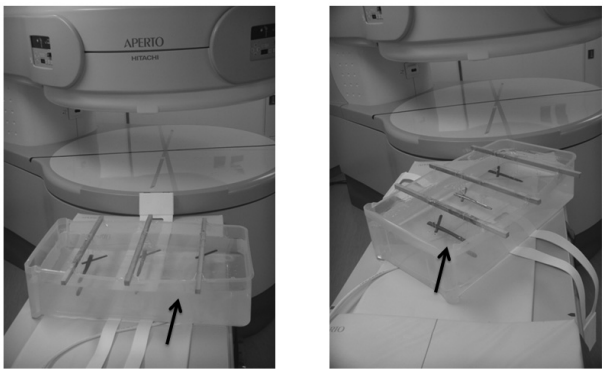

(a) (b)

Fig. 2 The relationship between the positioning of the device and the frequency-encoding gradient.
(a) The long axis of the rod is parallel to the frequency-encoding gradient. (b) The long axis of the lag screw is parallel to the frequency-encoding gradient. The solid arrow shows the frequency-encoding gradient direction.

(H_2O : 16 L, Polyvinyl alcohol : 16 L, Sodium Tetraborate : 180 g) so as to be at a 0° angle of anteversion.

All materials including metallic devices are generally classified into three categories ; diamagnetism, paramagnetism, and ferromagnetism. Stainless steel devices are considered to belong to the category of ferromagnetic substances because of their high content of ferromagnetic materials, such as iron and nickel. The magnetic susceptibilities of iron and nickel are 218 cm^3/g, and 55 cm^3/g, respectively. In contast, titanium alloy belongs to the category of Pauli paramagnetic substances. Its magnetism is generated from the magnetic moment by the spinning of conductive electrons. The contents of the ferromagnetic materials in the titanium alloy in our study is low. Moreover, the magnetic susceptibility of the other ingredients in our study ranged from -0.086×10^{-6} cm^3/g to $90.5 \times 10^{-6} cm^3/g$. The gel phantom used in this study mainly consists of water and Polyvinyl alcohol, which is an organic materials. Therefore, it is considered to belong to the category of diamagnetism. In the magnetic field of MR imaging, the magnetic susceptibilities of either paramagnetic or diamagnetic materials are so small that they are generally of a limited influence.

MRI Protocol

A 0.4-Tesla permanent magnet of the open MR imaging system (APERTO, Hitachi Medical Co. Ltd., Tokyo, Japan) was used in our study. The system has two disc-shaped gantries. The distance between the upper and the lower gantry was 38 cm and the diameter of the gantry was 150 cm. The permanent magnets generate a static magnetic field from floor to ceiling. The phantom was initially positioned in such a fashion that the long axis of the intramedullary rod was parallel to the frequency-encoding gradient. The angle between the long axis of the lag screw and the frequency-encoding gradient was 50° (Group R). The phantom was subsequently placed at a 50° angle counterclockwise rotation relative to Group R (Group L). For Group L, MR images were obtained with the long axis of the lag screw was parallel to the frequency-encoding gradient (Fig. 2). T1-, T2-weighted fast spin-echo (FSE), short TI inversion recovery (STIR) long TE, and short TE pulse sequences were used to obtain coronal images of the devices. The sequence parameters in our study are shown in Table 1. Other imaging parameters, including a 32- cm field of view, 512 x 512 recon. matrix, and a 4-mm slice thickness, were common to all sequences. A linear line of interest was standardized as the center of the part of the rod in the sagittal midline images, and the coronal images sliced in this line were evaluated in all images. Next, a linear line of interest was standardized as the center of the part of the long axis of the lag screw in the coronal midline images, and the axial images sliced in this line were evaluated in all images.

Mechanism of artifact generation

Magnetic susceptibility artifact describes either the image degradation or signal distortion that occurs in the soft tissues adjacent to ferromagnetic materials during MR imaging. Ferromagnetic materials become magnetized when placed in a large bore superconducting magnet, create their own magnetic field and dramatically alter precession frequencies of protons in the adjacent tissues. Tissues adjacent to ferromagnetic components become influenced by the induced magnetic field of the ferromagnetic materials rather than the parent field, and therefore either fail to be processed or do so at a difficult frequency and

Table 1 Imaging parameters

Sequence type	TR (msec)	TE (msec)	TI (msec)	Bandwidth (kHz)	Echo. Factor
FSE T1WI	600	14	—	21.3	2
FSE T2WI	3000	120	—	27.4	11
STIR long TE	3500	120	110	21.3	7
STIR short TE	3500	20	110	21.3	8

FSE = fast spin-echo, T1WI = T1-weighted image, T2WI = T2-weighted image, STIR = short TI inversion recovery.

hence do not generate useful signals.

Magnetic susceptibility artifact is composed of two components. One component is the artifact induced magnetism in the ferromagnetic component itself. Moreover, this artifact consists of low-signal intensity artifacts (signal void) and linear high-signal intensity artifacts around the signal void (misregistration artifact)[3]. This part of the artifact results in a fixed field distortion. The other component is the artifact induced magnetism in protons adjacent to the component. This part of the artifact which induces magnetism in protons (water) adjacent to the component results in an expanding field, results in the gradual diffusion of protons into adjacent soft tissues and dephasing of spins adjacent to the metal component, thus extending the area of signal disruption over time, and this effect previously been described as susceptibility blooming[11]. Such susceptibility blooming is reflected as a low-signal intensity in an image. The signal void and susceptibility blooming are different in the physical process described above, however, the differentiation between them tends to differ in a image, therefore we quantified them as the sum of the low-signal intensity artifacts.

The definition of the border of the artifact

In order to quantify the borders of the magnetic susceptibility artifacts, the acquired MR images of the DICOM data objects were transformed to bitmap images using a computer software program (Image J 1.41o, National Institute of Health, USA) (Fig. 3, 4). The shades of these images were showed as a hierarchization in 256 gray scales using a computer software program (Adobe Photoshop Elements 5.0, Adobe Systems Inc, Tokyo, Japan). The low-signal intensity artifacts were defined as the mean value between the gray scale of the gel phantom and that of the lowest gray scale in the low-signal intensity artifacts. The misregistration artifact border was defined as the mean value between the gray scale of the gel phantom and that of the highest

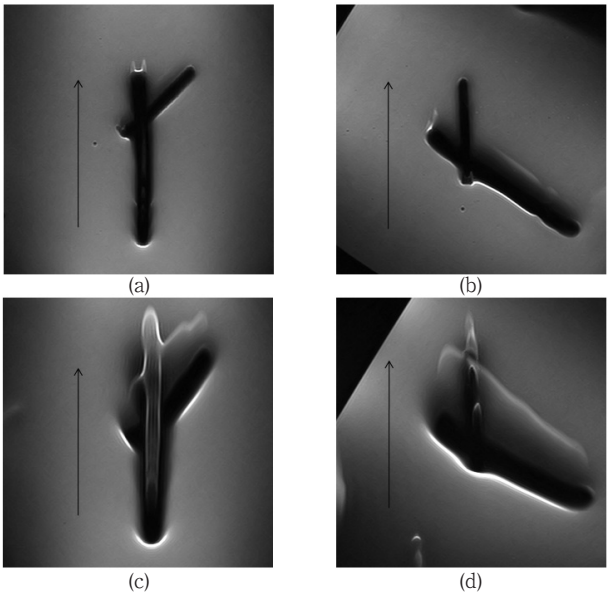

Fig. 3 The coronal T2-weighted fast spin-echo images (TR/TE : 3000/120 msec) of the titanium alloy ((a) Group R (b) Group L), and the stainless steel device ((c) Group R (d) Group L).
The titanium alloy device showed signal void, but little magnetic field distortion.
The stainless steel device showed large misregistration artifacts caused by magnetic field distortion.
The solid arrow shows the frequency-encoding gradient direction.

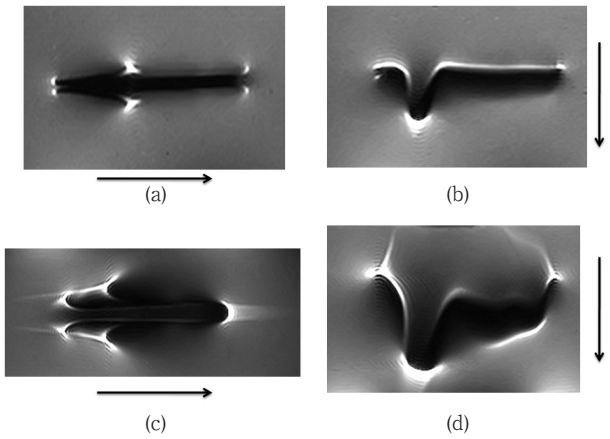

Fig. 4 The axial T2-weighted fast spin-echo images (TR/TE : 3000/120 msec) of the titanium alloy ((a) Group R (b) Group L), and the stainless steel device ((c) Group R (d) Group L).
Both devices showed less magnetic field distortion and misregistration artifacts when the frequency-encoding gradient is parallel to the long axis of the lag screw than when the frequency-encoding gradient is perpendicular to the long axis of the lag screw.
The solid arrow showed the frequency-encoding gradient direction.

(a) (b)

Fig. 5 The shade of the artifacts of the coronal T2-weighted fast spin-echo images of the stainless steel device in Group Rt.
(a) low-signal artifact. (b) high-signal artifact (misregistration artifact).

gray scale in the misregistration artifact. The shade of the misregistration artifact was reversed to black (Fig. 5). For example, in Figure 3 (c), the shade of the gel was 136 as a hierarchization in 256 gray scales, while that of the lowest gray scale of the low-signal intensity artifact was four. Therefore, the border of the low-signal intensity artifact was (136 + 4)/2 = 70. Furthermore, the shade of the highest gray scale in the misregistration artifact was 256, therefore the border of the high-signal intensity artifact was (136 + 256)/2 = 196. All of the images obtained in our study were calculated using a computer software program, because the gray scales of the gel, low-signal intensity area, and high-signal intensity area were slightly different in each image.

The pixel number of the artifact was calculated using another original computer software program, and the pixel number was converted into the area (the area of one pixel in our images was 0.625 x 0.625 mm^2). The sum of the low-signal intensity area and the high-signal intensity area was defined as the total area of the metallic susceptibility artifact. Furthermore, the actual areas of the devices in the coronal view and axial view were calculated using a computer software program (Adobe Photoshop Elements 5.0, Adobe Systems Inc, Tokyo, Japan).

Assessment of the artifact

The whole artifact area (Group Rt and Group Lt) and the limited area of the lag screw (Group Rl and Group Ll) were assessed in both groups. To compare the artifacts between the stainless steel and the titanium alloy, the artifact area in the Group Rt was also expressed as a percentage of the actual size of the angled cephalomedullary device. The images in all sequences were obtained five times in order to ensure the reliability of the values.

Statistical analysis

The values were presented as the mean and standard deviation for the mean. The areas were evaluated with Student's *t*-test for each group. The computer program JMP (SAS Institute, Cary, NC, USA) was used for the statistical analysis. Values of $p < 0.05$ were considered to be significant.

Results

The actual areas of the two devices

The actual areas of the stainless steel and the titanium alloy devices in the coronal plane were measured to be 32.87 cm^2 and 34.45 cm^2, respectively. The actual areas of the femoral neck lag screw of the stainless steel and the titanium alloy in the axial plane were measured to be 10.46 cm^2 and 11.19 cm^2, respectively.

The comparison of the artifact areas between the two devices in the coronal plane

The percentage of the artifact areas is shown in Table 2. In the titanium alloy device, the mean artifact size ranged from 142.6% to 154.5% of the actual size of the device. In the stainless steel device, the mean artifact size ranged from 247.0% to 288.9% of the actual size of the device. The titanium alloy device showed significantly smaller artifact area than the stainless steel device in all sequences ($p < 0.05$; Student's *t*-test).

The artifact areas of these devices with the three pulse sequences are shown in Table 3. The

artifact area of Group Lt was significantly larger than that of Group Rt in all sequences ($p < 0.05$; Student's *t*-test). However, the artifact area of Group Ll was significantly smaller than that of Group Rl in all sequences ($p < 0.05$; Student's *t*-test).

The comparison of the artifact areas between the two devices in the axial plane

The artifact areas of these devices with the three pulse sequences are shown in Table 4. In both devices, the artifacts with the long axis of the lag screw parallel to the frequency-encoding gradient were significantly smaller than those with the long axis of the lag screw perpendicular to the frequency-encoding gradient in all sequences ($p < 0.05$; Student's *t*-test).

Discussion

The main findings of this study demonstrated that the optimal method for reducing artifacts is adjusting the long axis of the regions of interest parallel to the frequency-encoding gradient, even for an angled cephalomedullary device of the proximal femur. We focused on the relationship between the orientation of the angled cephalomedullary device and the frequency-encoding gradient direction. The FOV was uniform in all pulse sequences, and the read-out gradient bandwidth was uniform in all pulse sequences other than T2WI in our study. The reason is that by making these two parameters constant, we could acquire only the change in the metallic susceptibility artifact induced by the orientating

Table 2 The percentage of the artifact areas in Group Rt to the actual areas (%)

Implant type	FSE T1WI	FSE T2WI	STIR long TE	STIR short TE
Titanium alloy	152.2 ± 3.5*	142.6 ± 3.1*	150.9 ± 1.7*	154.5 ± 3.7*
Stainless steel	247.0 ± 2.6	248.8 ± 2.3	278.9 ± 4.0	288.9 ± 5.9

The values are shown as the mean ± standard deviation for the mean. The titanium alloy device had significantly smaller artifacts than the stainless steel device in all sequences (*$p < 0.05$; Student's *t*-test).
FSE = fast spin-echo, STIR = short TI inversion recovery

Table 3 The artifact area of each group in the coronal view (cm^2)

		FSE T1WI	FSE T2WI	STIR short TE	STIR long TE
Titanium alloy	Rt	52.5 ± 1.2	49.1 ± 1.1	53.2 ± 1.3	52.0 ± 0.6
	Lt	55.1 ± 1.5*	55.4 ± 1.4*	57.5 ± 0.8*	56.4 ± 1.3*
	Rl	18.1 ± 0.8	17.4 ± 0.9	19.6 ± 1.0	18.8 ± 0.9
	Ll	14.4 ± 0.5†	13.7 ± 0.9†	14.4 ± 0.4†	14.3 ± 0.7†
Stainless steel	Rt	81.2 ± 0.9	81.8 ± 0.8	95.0 ± 1.9	91.7 ± 1.3
	Lt	89.7 ± 0.7*	93.5 ± 1.4*	105.1 ± 1.6*	102.3 ± 1.6*
	Rl	39.0 ± 1.9	40.9 ± 1.1	48.4 ± 2.1	46.8 ± 3.5
	Ll	32.5 ± 2.1†	28.7 ± 1.4†	34.0 ± 1.0†	33.3 ± 1.6†

The values are shown as the mean ± standard deviation for the mean. The artifact area of the group Lt was significantly larger than that of group Rt in all sequences (*$p < 0.05$; Student's *t*-test). In contrast, the artifact area of group Ll was significantly smaller than that of group Rl in all sequences (†$p < 0.05$; Student's *t*-test).
FSE = fast spin-echo, STIR = short TI inversion recovery

Table 4 The artifact area of each group in the axial view (cm^2)

Frequency-encoding direction	FSE T1WI	FSE T2WI	STIR short TE	STIR long TE
Titanium paralell	11.9 ± 0.7	12.9 ± 0.5	13.3 ± 1.2	13.3 ± 0.8
Titanium perpendicular	15.7 ± 0.5*	16.5 ± 1.2*	17.9 ± 0.7*	18.0 ± 0.6*
Stainless paralell	45.9 ± 2.3	46.8 ± 0.8	43.2 ± 2.0	43.8 ± 3.0
Stainless perpendicular	50.1 ± 0.9†	49.9 ± 0.8†	53.7 ± 1.8†	52.1 ± 1.3†

The values are shown as the mean ± standard deviation for the mean. The artifact area when the frequency-encoding gradient was parallel to the long axis of the lag screw was significantly smaller than that of when the frequency-encoding gradient was perpendicular to the long axis of the lag screw was in all sequences (*$p < 0.05$; Student's *t*-test).
FSE = fast spin-echo, STIR = short TI inversion recovery

devices. In the titanium alloy device, the mean artifact area in Group Ll was 21% smaller than that in Group Rl, although the mean artifact area in Group Lt was 13 % larger than Group Rt on the coronal T2-weighted FSE images. In the stainless steel device, the mean artifact area in Group Ll was also 30% smaller than that in Group Rl, although the mean artifact area in Group Lt was 14% larger than that in Group Rt on the coronal T2-weighted FSE images. The results therefore indicated that our hypothesis was valid.

The images of the device were generally obtained with the short intramedullary rod parallel to the frequency-encoding gradient, because the short intramedullary rod is the main component of this device and is inserted along the long axis of the femur. In our study, the gel phantom was placed at a 50° angle in an counterclockwise rotation to the initial position, and the long axis of the lag screw was subsequently set to be parallel to the frequency-encoding gradient. By means of this method, the magnetic susceptibility artifacts of the lag screw could be reduced. For example, to minimize the artifact of the lag screws which were inserted into the right side of the femur, we could reveal that the lower extremities should be placed at a 50° angle in an anticlockwise rotation to the usual patient position in our open MR imaging.

Many strategies have been reported for reducing the size of susceptibility artifacts. These strategies have included the composition of the implant[2)8)9)12)~20)], MR imaging sequence adjustments and techniques[3)6)8)11)21)~25)], and patient position[4)~10)26)]. The conventional high-field closed bore MRI systems restrict patient positioning for most orthopaedic devices. For example, patients who experience contracture or pain in their hip joint tend to have a restricted range of motion. In the conventional closed-bore MRI, this optimal position is impossible because the normal human maximum adduction angle of the hip joint is 20°. In contrast, open MR imaging provides much flexibility for patient positioning, and the body is freely moved in one plane so that the frequency-encoding gradient is parallel to the regions of interest[8)27)]. Harris et al.[27)] reported the importance of patient positioning in the MR imaging to reduce the susceptibility artifacts, and emphasized that the limitation in patient positioning resulting from restrictive MR imaging scanner bore diameters could be overcome in magnets with an open configuration. We demonstrated that our open MR imaging enables the body position to be freely adjusted according to the device shape.

The quantification of magnetic susceptibility artifact has been performed in several studies[9)10)17)21)24)25)28)]. However, few studies have so far carried out the quantification of the artifact area or a subsequent statistical analysis of that area[10)]. In our study, the artifact areas of the images for each sequence type were calculated five times, and each was set at their own standard line in the saggital plane. Moreover, to define the artifact borders objectively, we used shades of the artifact that were hierarchized as 256 gray scales by a computer software program. This method allowed us to standardize and quantify the so-called 'vague' artifact.

It is important to establish measures for metallic implants in human body during MRI examinations. Heat production and magnetic attraction are the problems to the patients inserted the metallic devices. Orthopaedic metallic implants are said to be safe to the MRI examinations[29)30)]. However, stainless steels have more possibility to cause these side effects, therefore, it is necessary to perform the MRI examination in a short time, to use a low magnetic field scanner, and the observation of safety guidelines for metallic implants.

One limitation of the current study was that, in our method, it was difficult for us to differentiate the susceptibility artifact from ferromagnetic artifacts, paramagnetic, and metal artifacts from the induced currents affecting the rf field. The reason was that we decided the border of the

artifact as hierarchization in the 256 gray scales, and calculated the sum of the black and white zone as a so-called artifact. However, both the susceptibility artifact and ferromagnetic or paramagnetic artifacts are similar in regard to the fact that they interfere with evaluations of the surrounding tissue. We therefore quantified the sum of the susceptibility artifacts and metal artifacts as so-called magnetic susceptibility artifacts.

Another limitation was that we examined only two kinds of positioning of the device. Therefore, we could only demonstrate if the regions of interest were around the lag screw, the device should be adjusted with the lag screw parallel to the frequency-encoding gradient direction, rather than with the main intramedullary rod parallel to the frequency-encoding gradient direction.

In conclusion, magnetic susceptibility artifacts for an angled cephalomedullary device of the proximal femur could be minimized when the long axis of the regions of interest is parallel to the frequency-encoding gradient direction. For minimizing the magnetic susceptibility artifacts, open MR imaging therefore enables us to obtain the optimal orientation which is normally extremely difficult to establish when using conventional closed MR imaging.

Acknowledgments

We acknowledge Junji Kishimoto, PhD, for providing excellent statistical advice.

References

1) Augustiny N, von Schulthess GK, Meier D and Bösiger P : MR imaging of large nonferromagnetic metallic implants at 1.5 T. J Comput Assist Tomogr. 11 : 678-683, 1987.
2) Ebraheim NA, Savolaine ER, Zeiss J and Jackson WT : Titanium hip implants for improved magnetic resonance and computed tomography examinations. Clin Orthop Relat Res. 275 : 194-198, 1992.
3) White LM, Kim JK, Mehta M, Merchant N, Schweitzer ME, Morrison WB, Hutchison CR and Gross AE : Complications of total hip arthroplasty : MR imaging-initial experience. Radiology. 215 : 254-262, 2000.
4) Lüdeke KM, Röschmann P and Tischler R : Susceptibility artefacts in NMR imaging. Magn Reson Imaging. 3 : 329-343, 1985.
5) Oehler MC, Schmalbrock P, Chakeres D and Kurucay S : Magnetic susceptibility artifacts on high-resolution MR of the temporal bone. AJNR Am J Neuroradiol. 16 : 1135-1143, 1995.
6) Törmänen J, Tervonen O, Koivula A, Junila J and Suramo I : Image technique optimization in MR imaging of a titanium alloy joint prosthesis. J Magn Reson Imaging. 6 : 805-811, 1996.
7) Eustace S, Goldberg R, Williamson D, Melhem ER, Oladipo O, Yucel EK and Jara H : MR imaging of soft tissues adjacent to orthopaedic hardware : techniques to minimize susceptibility artefact. Clin Radiol. 52 : 589-594, 1997.
8) Suh JS, Jeong EK, Shin KH, Cho JH, Na JB, Kim DH and Han CD : Minimizing artifacts caused by metallic implants at MR imaging : experimental and clinical studies. AJR Am J Roentgenol. 171 : 1207-1213, 1998.
9) Ganapathi M, Joseph G, Savage R, Jones AR, Timms B and Lyons K : MRI susceptibility artefacts related to scaphoid screws : the effect of screw type, screw orientation and imaging parameters J Hand Surg Br. 27 : 165-170, 2002.
10) Frazzini VI, Kagetsu NJ, Johnson CE and Destian S : Internally stabilized spine : optimal choice of frequency-encoding gradient direction during MR imaging minimizes susceptibility artifact from titanium vertebral body screws. Radiology. 204 : 268-272, 1997.
11) Arbogast-Ravier S, Gangi A, Choquet P, Brunot B and Constantinesco A : An in vitro study at low field for MR guidance of a biopsy needle. Magn Reson Imaging. 13 : 321-324, 1995.
12) Ebraheim NA, Savolaine ER, Stitgen SH and Jackson WT : Magnetic resonance imaging after pedicular screw fixation of the spine. Clin Orthop Relat Res. 279 : 133-137, 1992.
13) Rupp R, Ebraheim NA, Savolaine ER and Jackson WT : Magnetic resonance imaging evaluation of the spine with metal implants. General safety and superior imaging with titanium. Spine. 18 : 379-385, 1993.
14) Burtscher IM, Owman T, Romner B, Stählberg F and Holtäs S : Aneurysm clip MR artifacts. Titanium versus stainless steel and influence of imaging parameters. Acta Radiol. 39 : 70-76, 1998.
15) Rudisch A, Kremser C, Peer S, Kathrein A,

Judmaier W and Daniaux H : Metallic artifacts in magnetic resonance imaging of patients with spinal fusion. A comparison of implant materials and imaging sequences. Spine. 23 : 692-699, 1998.
16) Shellock FG and Kanal E : Aneurysm clips : evaluation of MR imaging artifacts at 1.5 T. Radiology. 209 : 563-566, 1998.
17) Verheyden P, Katscher S, Schulz T, Schmidt F and Josten C : Open MR imaging in spine surgery : experimental investigations and first clinical experiences. Eur Spine J. 8 : 346-353, 1999.
18) Ebraheim NA, Rupp RE, Savolaine ER and Reinke D : Use of titanium implants in pedicular screw fixation. J Spinal Disord. 7 : 478-486, 1994.
19) Kato Y, Sano H, Katada K et al : Effects of new titanium cerebral aneurysm clips on MRI and CT images. Minim Invasive Neurosurg. 39 : 82-85, 1996.
20) Wichmann W, Von Ammon K, Fink U, Weik T and Yasargil GM : Aneurysm clips made of titanium : magnetic characteristics and artifacts in MR. AJNR Am J Neuroradiol. 18 : 939-944, 1997.
21) Petersilge CA, Lewin JS, Duerk JL, Yoo JU and Ghaneyem AJ : Optimizing imaging parameters for MR evaluation of the spine with titanium pedicle screws. AJR Am J Roentgenol. 166 : 1213-1218, 1996.
22) Tartaglino LM, Flanders AE, Vinitski S and Friedman DP : Metallic artifacts on MR images of the postoperative spine : reduction with fast spin-echo techniques. Radiology. 190 : 565-569, 1994.
23) Eustace S, Jara H, Goldberg R, Fenlon H, Mason M, Melhem ER and Yucel EK : A comparison of conventional spin-echo and turbo spin-echo imaging of soft tissues adjacent to orthopedic hardware. AJR Am J Roentgenol. 170 : 455-458, 1998.
24) Lee MJ, Janzen DL, Munk PL, MacKay A, Xiang QS and McGowen A : Quantitative assessment of an MR technique for reducing metal artifact : application to spin-echo imaging in a phantom. Skeletal Radiol. 30 : 398-401, 2001.
25) Kolind SH, MacKay AL, Munk PL and Xiang QS : Quantitative evaluation of metal artifact reduction techniques. J Magn Reson Imaging. 20 : 487-495, 2004.
26) Guermazi A, Miaux Y, Zaim S, Peterfy CG, White D and Genant HK : Metallic artefacts in MR imaging : effects of main field orientation and strength. Clin Radiol. 58 : 322-328, 2003.
27) Harris CA and White LM : Metal artifact reduction in musculoskeletal magnetic resonance imaging. Orthop Clin North Am. 37 : 349-359, 2006.
28) Matsuura H, Inoue T, Ogasawara K, Sasaki M, Konno H, Kuzu Y, Nishimoto H and Ogawa A : Quantitative analysis of magnetic resonance imaging susceptibility artifacts caused by neurosurgical biomaterials : comparison of 0.5, 1.5, and 3.0 Tesla magnetic fields. Neurol Med Chir (Tokyo). 45 : 395-398 ; discussion 398-399, 2005.
29) Kanal E, Borgstede JP, Barkovich AJ, Bell C, Bradley WG, Felmlee JP, Froelich JW, Kaminski EM, Keeler EK, Lester JW, Scoumis EA, Zaremba LA and Zinninger MD : American College of Radiology : White Paper on MR Safety. Am J Roentgenol, 178 : 1335-1347, 2002.
30) Shellock FG, and Crues JV 3rd.: MR Safety and the American College of Radiology White Paper. Am J Roentgenol, 178 : 1349-1352, 2002.

(Received for publication January 25, 2011)

（和文抄録）

大腿骨近位部骨折用髄内釘の金属方向と周波数エンコード傾斜磁場の方向は，磁化率アーチファクトの出現に影響を与える：open MRI を用いた検討

[1)]九州大学大学院医学研究院 整形外科
[2)]日立メディコ株式会社 アプリケーション部
[3)]九州産業大学 工学部 バイオロボティクス学科
[4)]九州大学先端医工学部診療部

竹内直英[1)]，光安廣倫[1)]，仲西知憲[1)]，西村須磨子[2)]，
下戸 健[3)]，日垣秀彦[3)]，橋爪 誠[4)]，岩本幸英[1)]

目的：整形外科骨接合術材料（以下，インプラント）の周囲に発生する MRI の磁化率アーチファクトを定量化し，周波数エンコード傾斜磁場の方向の違いによる磁化率アーチファクトの発生について検討することである．

対象と方法：２種類の大腿骨近位部骨折用の髄内釘（ステンレス製，チタン製）をゲルファントム内に固定した後に，0.4 Tesla open MRI（APERTO：日立メディコ社製）を用いて撮影した．まず，インプラントの rod 部分の長軸に平行になるように周波数エンコード傾斜磁場の方向を設定して撮影した（Group R）．次に lag screw 部分の長軸に平行になるように周波数エンコード傾斜磁場の方向を設定して撮影した（Group L）．インプラント全体の磁化率アーチファクトと lag screw 周囲のみの磁化率アーチファクトの面積を前額面と lag screw の長軸に沿った横断面で測定し，両群間で比較検討した．統計学的検討は Student's *t*-test を用い，$p < 0.05$ を有意水準とした．

結果：磁化率アーチファクトの面積は，ステンレス製，チタン製共に，Group L は Group R よりも有意に大きかったが，lag screw 部分のみに限定した場合は，Group L は Group R よりも有意に小さかった（$p < 0.05$）．

考察：大腿骨近位部骨折用の骨接合材料のような角度付きインプラントにおいて，磁化率アーチファクトを減少させるためには，目的の部分の金属方向に周波数エンコード傾斜磁場の方向を平行に設定することが重要である．また，Open MRI は体位を自由に変えることができるため，磁化率アーチファクトを最小にする至適な位置を得ることが可能であることが示唆された．